

HELIUM CORE WHITE DWARFS IN CATAclySMIC VARIABLES

KEN J. SHEN¹, IRIT IDAN^{2,3}, AND LARS BILDSTEN^{1,4}

Draft version October 26, 2018

ABSTRACT

Binary evolution predicts a population of helium core ($M < 0.5 M_{\odot}$) white dwarfs (WDs) that are slowly accreting hydrogen-rich material from low mass main sequence or brown dwarf donors with orbital periods less than four hours. Four binaries are presently known in the Milky Way that will reach such a mass-transferring state in a few Gyr. Despite these predictions and observations of progenitor binaries, there are still no secure cases of helium core WDs among the mass-transferring cataclysmic variables (CVs). This led us to calculate the fate of He WDs once accretion begins at a rate $\dot{M} < 10^{-10} M_{\odot} \text{ yr}^{-1}$ set by angular momentum losses. We show here that the cold He core temperatures ($T_c < 10^7$ K) and low \dot{M} result in $\sim 10^{-3} M_{\odot}$ of accumulated H-rich material at the onset of the thermonuclear runaway. Shara and collaborators noted that these large accumulated masses may lead to exceptionally long classical nova (CN) events. For a typical donor star of $0.2 M_{\odot}$, such binaries will only yield a few hundred CNe, making these events rare amongst all CNe. We calculate the reheating of the accreting WD, allowing a comparison to the measured WD effective temperatures in quiescent dwarf novae and raising the possibility that WD seismology may be the best way to confirm the presence of a He WD. We also find that a very long (> 1000 yr) stable burning phase occurs after the CN outburst, potentially explaining enigmatic short orbital period supersoft sources like RX J0537-7034 ($P_{\text{orb}} = 3.5$ hr) and 1E 0035.4-7230 ($P_{\text{orb}} = 4.1$ hr).

Subject headings: accretion, accretion disks — binaries: close — nuclear reactions, nucleosynthesis, abundances — novae, cataclysmic variables — stars: dwarf novae — white dwarfs

1. INTRODUCTION

For short enough orbital periods, the evolution of a low-mass star in a binary system up the red giant branch can be halted by the onset of catastrophic filling of its Roche lobe. This exposes the low-mass ($M < 0.5 M_{\odot}$; e.g., Dominguez et al. 1999; Salaris et al. 2002; Serenelli & Fukugita 2005) helium core of the red giant and triggers a common envelope event (see Sandquist et al. 2000 for an overview) that brings the resulting cooling He white dwarf (WD) much closer to its stellar companion (de Kool 1992; de Kool & Ritter 1993; Iben & Tutukov 1993). The discovery by Marsh et al. (1995) that low-mass WDs have stellar companions supports this origin for many He core WDs.

Angular momentum losses (either from gravitational waves or stellar wind braking) after the common envelope event will drive the binary closer, with some reaching contact in a few Gyr to become cataclysmic variables (CVs). Schreiber & Gänsicke (2003) studied such pre-CVs, noting that a few have He WDs. The recently discovered system WD 0137-349 is a new pre-CV example with a $0.39 M_{\odot}$ WD and a $0.053 M_{\odot}$ brown dwarf companion that will come into contact in 1.4 Gyr (Maxted et al. 2006). Population synthesis calculations (de Kool 1992; Politano 1996; Howell et al. 2001) predict that as many as $\approx 20\%$ of CVs with orbital periods $P_{\text{orb}} < 2$ hr should have He WDs. However,

where WD masses are inferred in CVs (Patterson 2001; Townsley & Gänsicke 2009), no such low masses have been identified.

These considerations led Shara et al. (1993) to examine classical nova (CN) events in these unusual systems. They calculated the outcomes for a $0.4 M_{\odot}$ He WD accreting at a rate of $\dot{M} = 10^{-9} M_{\odot} \text{ yr}^{-1}$, finding accumulated masses of $M_{\text{ign}} = 9 \times 10^{-4} M_{\odot}$ for a WD core temperature of $T_c = 10^7$ K and a time between outbursts of 10^6 yr. They evolved the WD for nine flashes, finding slow novae followed by a prolonged bright ($L > 10^3 L_{\odot}$) phase after the outburst, as the residual $\approx 10^{-4} M_{\odot}$ hydrogen shell burns stably. The combination of a large M_{ign} in a tight binary may make these events exceptional. In the case of C/O WDs, Iben & Tutukov (1992) suggested that such events would trigger a common envelope event of some significance, potentially explaining the very bright “red variable” seen in M31 (Rich et al. 1989; Boschi & Munari 2004).

The known pre-CVs with He WDs provide excellent starting points for our work, so we begin in §2 by noting the stability of mass transfer once contact is reached and deriving the subsequent $\dot{M}(t)$ histories. We find that lower accretion rates than studied by Shara et al. (1993) need to be considered, so in §3 we perform (and analyze) a few Gyr of time evolution at constant low $\dot{M} = 10^{-10} M_{\odot} \text{ yr}^{-1}$ and $10^{-11} M_{\odot} \text{ yr}^{-1}$ on a $0.4 M_{\odot}$ He WD. Given the low \dot{M} , there is time for diffusion to occur between the fresh material and the WD (Paquette et al. 1986; Iben et al. 1992), which we discuss in the Appendix.

In §4, we perform calculations of two specific scenarios motivated by the known He WD pre-CVs. Our focus

¹ Department of Physics, Broida Hall, University of California, Santa Barbara, CA 93106

² Rafael, 31021 Haifa, Israel

³ Department of Physics, Technion-Israel Institute of Technology, 32000 Haifa, Israel

⁴ Kavli Institute for Theoretical Physics, Kohn Hall, University of California, Santa Barbara, CA 93106

there is on the long-term evolution of their CN outbursts as well as the T_c evolution. We also discuss the WD surface temperatures when in quiescence as dwarf nova systems and the potential discovery of He WDs through their pulsations (Arras et al. 2006). In §5, we explore details of the individual novae, describing the physics of the convective burning phase in §5.1, and the composition of the nova ejecta in §5.2, which is not enhanced in CNO nuclei due to the lack of a reservoir of underlying C/O as in normal CNe (Starrfield et al. 1972; Gehrz et al. 1998). The CN event leaves a remnant burning envelope on the surface of the WD, allowing for a prolonged stable burning phase (Shara et al. 1993) that we detail in §5.3, which may explain the few $P_{\text{orb}} \lesssim 4$ hr long-lived supersoft sources (SSSs). We conclude in §6 by highlighting where future CV and CN observations may reveal the long-lost helium core WDs in mass transferring binaries.

2. STABLE MASS TRANSFER RATES

The common envelope event that exposes the He WD leaves a wide range of WD and donor masses (M_d), only a fraction of which will become stable mass-transferring binaries once the donor comes into contact (de Kool 1992; Politano 1996; Howell et al. 2001). Table 1 shows the parameters of those pre-CVs with probable He WDs whose companions will overflow their Roche lobes in $t_{\text{in}} < 20$ Gyr, under the assumption of angular momentum losses due to gravitational waves. The prevalence of low-mass ($M_d < 0.25 M_\odot$) main sequence companions is likely due to their slower inspiral under gravitational wave losses compared to those with more massive ($M_d > 0.25 M_\odot$) companions that would have stellar wind braking (Schreiber & Gänsicke 2003). As we will show in the following sections, all binaries in Table 1 will likely transfer matter stably after contact, leading to the accretion of cosmic-mix material onto a He WD at $\dot{M} = 1 - 4 \times 10^{-11} M_\odot \text{ yr}^{-1}$.

2.1. Stability of Mass Transfer

When the main sequence star comes into contact, the possibility exists for dynamically unstable mass transfer, which occurs when the donor's Roche radius shrinks faster or expands slower than the donor's radial response to adiabatic changes (Webbink 1985; Hjellming & Webbink 1987). Low-mass main sequence stars have small radiative cores and large convective envelopes that make up $> 50\%$ of the star's mass, and stars with $M_d < 0.3 M_\odot$ are nearly fully convective. The adiabatic response of the radius of a fully convective star to mass loss is $d \ln R_d / d \ln M_d|_s = -1/3$, and using the Paczyński (1967) approximation to the donor's Roche radius yields $d \ln R_L / d \ln M_d = -5/3 + 2q$, where $q \equiv M_d/M$. Thus, dynamically unstable mass transfer occurs if the donor is fully convective and has a mass ratio $M_d/M > 2/3$. For the maximum mass He WD with $M = 0.5 M_\odot$, this restricts the main sequence donor mass to $M_d < 0.33 M_\odot$ in order to avoid dynamical mass transfer. If the more exact Roche radius formula from Eggleton (1983) is used, the limit changes only slightly to $M_d/M < 0.63$. Binaries just at the limit of stability would have donors that fill their Roche lobes as main sequence stars ($M_d = 0.33 M_\odot$, $R_d = 0.33 R_\odot$; Ribas et al. 2008) with $P_{\text{orb}} = 3$ hr. Any bloating of such a donor

could drive P_{orb} slightly longer, potentially to the 3.5–4 hr seen in a few supersoft sources, as we discuss in §5.3.

All the pre-CVs in Table 1 have $M_d/M \lesssim 0.63$ and will become stable mass transfer systems when they come into contact a time t_{in} from now. We derive their mass transfer rates in §2.2. There are certainly He WD post-common envelope systems with less extreme mass ratios that would trigger a dynamical mass transfer event at the onset of Roche lobe filling. These yield a red giant configuration, as the supply of freshly accreted H leads to a rejuvenation of the H burning shell typical of a He core on the first ascent of the red giant branch.

2.2. Mass Transfer Rates for Stable Scenarios

Our focus here is on those systems that undergo stable mass transfer, with the WD accumulating mass over time and then ejecting most of it during the CN. We start with a total mass $M_t = M_d + M$ and orbital angular momentum $J = M_d M (Ga/M_t)^{1/2}$ for an orbital separation a . Mass transfer is driven by the rate of orbital angular momentum loss, \dot{J} , via

$$\frac{\dot{J}}{J} = \frac{\dot{M}_d}{M_d} + \frac{\dot{M}}{M} + \frac{1}{2} \frac{\dot{a}}{a} - \frac{1}{2} \frac{\dot{M}_t}{M_t}. \quad (1)$$

Since CNe lead to ejection of material from the binary, we must account for mass loss. We define an excavation factor f by setting $\dot{M}_t = f \dot{M}_d$, so that $f = 1$ means the WD, on average, keeps a constant mass (i.e., the CNe eject the amount of matter that is accreted), and $f = 0$ means that the WD keeps all the accreted mass. The resulting relation is then

$$\frac{\dot{J}}{J} = \frac{\dot{M}_d}{M_d} \left[1 + \frac{(f-1)M_d}{M} - \frac{f M_d}{2 M_t} \right] + \frac{1}{2} \frac{\dot{a}}{a}. \quad (2)$$

Presuming that the donor always fills its Roche lobe, and using the Paczyński (1967) formulation, we obtain

$$\frac{\dot{J}}{J} = \frac{1}{2} \frac{\dot{R}_d}{R_d} + \frac{\dot{M}_d}{M_d} \left[\frac{5}{6} + \frac{(f-1)M_d}{M} - \frac{f M_d}{3 M_t} \right]. \quad (3)$$

We need the response of the donor star's radius to mass loss, $\zeta_d = d \ln R_d / d \ln M_d$, which initially occurs on a timescale longer than the Kelvin-Helmholtz time, allowing the star to stay close to the main sequence (e.g., $\zeta_d \approx 1$). However, the increase of the Kelvin-Helmholtz time as M_d decreases leads to a nearly adiabatic response ($\zeta_d \approx -1/3$) late in the binary evolution (Kolb & Baraffe 1999).

The resulting mass transfer rate is then

$$\frac{\dot{J}}{J} = \frac{\dot{M}_d}{M_d} \left[\frac{5}{6} + \frac{\zeta_d}{2} + \frac{(f-1)M_d}{M} - \frac{f M_d}{3 M_t} \right], \quad (4)$$

where we use the work of Kolb & Baraffe (1999) to obtain $R_d(M_d)$ and ζ_d . Their $R_d(M_d)$ relation was calculated self-consistently for a $M = 0.6 M_\odot$ WD with gravitational wave losses alone. We also presume that gravitational-wave losses set \dot{J} and consider a few specific scenarios in Figure 1. The two solid lines labeled A and B are the two scenarios we will discuss at length in §4. Scenario A begins with a $M_d = 0.2 M_\odot$ donor, while scenario B begins with a $M_d = 0.05 M_\odot$ donor. Both assume that all matter accreted onto the WD is ejected

TABLE 1
HELIUM WD PRE-CVs WITH $t_{\text{in}} < 20$ Gyr (AS OF JULY 2009)

System	M (M_{\odot})	M_d (M_{\odot})	t_{in} (Gyr)	Ref.
SDSS J1435+3733	0.48 – 0.53	0.19 – 0.25	0.75 – 1.1	1,2
HR Cam (GD 448)	0.41 ± 0.01	0.096 ± 0.004	1.5 – 2.1	3
WD 0137-349	0.39 ± 0.035	0.053 ± 0.006	1.7 – 2.5	4
SDSS J1529+0020	0.40 ± 0.04	0.25 ± 0.12	0.54 – 6.3	5
SDSS J0110+1326	0.47 ± 0.2	0.255 – 0.38	12 – 19	2
SDSS J1724+5620	0.42 ± 0.01	0.25 – 0.38	13 – 20	5
RR Cae	0.44 ± 0.022	0.182 ± 0.013	18 – 23	6
SDSS J1212-0123	0.33 – 0.48	0.26 ± 0.03	16 – 26	7

1. Steinfadt et al. (2008), 2. Pyrzas et al. (2009), 3. Maxted et al. (1998), 4. Maxted et al. (2006), 5. Rebassa-Mansergas et al. (2008), 6. Maxted et al. (2007), 7. Nebot Gómez-Morán et al. (2009)

during the CN event. The resulting accretion rates are $< 4 \times 10^{-11} M_{\odot} \text{ yr}^{-1}$ once mass transfer begins. The trends that we discuss throughout the rest of the paper for $0.2 M_{\odot}$ donors will apply to larger donors as well because the accretion rates determined by gravitational wave radiation for low-mass main-sequence donors differ by a factor of a few at most. For example, the accretion rate for the most massive stably mass-transferring system ($M_d = 0.33 M_{\odot}$, $M = 0.5 M_{\odot}$) is only 3 times larger at a given orbital period than our fiducial example with $M_d = 0.2 M_{\odot}$ and $M = 0.4 M_{\odot}$.

We neglect any potential variations of \dot{M} on the CN recurrence time due to prolonged periods of “hibernation” (Shara et al. 1986). We further note that the $R_d(M_d)$ relation we use assumes a donor with solar metallicity. As Stehle et al. (1997) and Kolb & Baraffe (1999) note, the secondary’s composition does have an effect on its structure and thus on the secular evolution of the CV. We have also neglected the small correction needed to re-adjust the $R_d(M_d)$ relation for our specific \dot{M} history, which is lower by a factor of ≈ 1.5 than that in Kolb & Baraffe (1999) due to our $0.4 M_{\odot}$ WD (they modeled a $0.6 M_{\odot}$ WD). This would tend to slightly shorten the minimum orbital period, as the mass-transfer timescale at a given donor mass is longer in our case. However, given that the current calculations do not match the now observed minimum orbital period in either case (Gänsicke et al. 2009), we will neglect the corrections due to the secondary’s composition and \dot{M} history.

3. REHEATING OF SLOWLY ACCRETING HELIUM WHITE DWARFS

The previous section showed that the relevant accretion rates are much lower than that considered by Shara et al. (1993). In addition, by the time the known pre-CVs come into contact and initiate stable mass transfer, the He WD core will have cooled to $T_c \approx 2 - 6 \times 10^6$ K (Althaus & Benvenuto 1997). Extensions of the work by Townsley & Bildsten (2004) on CN ignition masses to lower M , \dot{M} and T_c yields $M_{\text{ign}} \approx 10^{-3} M_{\odot}$. This implies CN recurrence times of $10^7 - 10^8$ yr during the many gigayears of evolution under accretion. The long evolution time allows for significant thermal coupling between the freshly accreted H envelope and the He WD core during the accumulation of fresh matter. For this reason, we must track T_c and its evolution under the action of accretion for a prolonged period of hundreds of

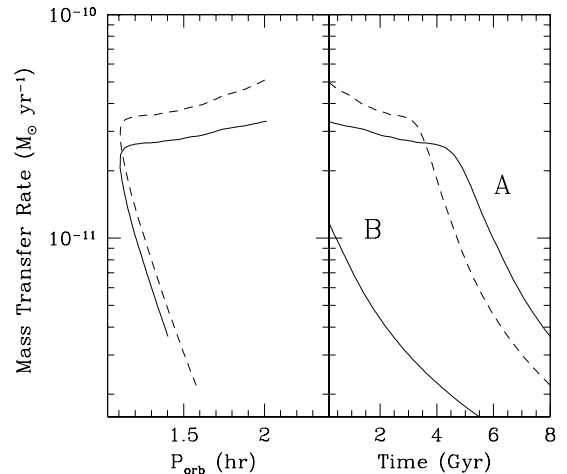


FIG. 1.— The solid line in the left panel shows \dot{M} as a function of P_{orb} assuming that all mass accreted onto the $0.4 M_{\odot}$ WD is ejected by CNe ($f = 1$) for an initial $M_d = 0.2 M_{\odot}$ donor (scenario A; e.g., SDSS J1529+0020). The dashed line assumes that all accreted matter stays on the WD ($f = 0$). The upper solid and dashed lines in the right-hand panel show the corresponding $\dot{M}(t)$ profiles. The lower solid curve in the right hand panel shows \dot{M} for a donor with initial $M_d = 0.05 M_{\odot}$ (e.g., WD 0137-349), assuming that CNe eject all the accreted material ($f = 1$; scenario B).

CN events.

3.1. Analytic estimate of thermal coupling between the envelope and core

Due to the long accumulation and evolution time, much of the He WD core participates in the thermal balance of the CN cycle. We begin by estimating the timescale for heat transport between two mass shells at radial coordinates r_0 and r (Heneyey & L’Ecuyer 1969),

$$\tau_d \approx \frac{3}{16a_{\text{SB}}c} \left[\int_{r_0}^r \left(\frac{\kappa c_P}{T^3} \right)^{1/2} \rho dr \right]^2, \quad (5)$$

where c_P is the specific heat, a_{SB} is the Stefan-Boltzmann radiation constant, and κ is the opacity. Electron conduction determines heat transfer in the degenerate He core, so $\kappa = \kappa' T^2 / \rho^2$, where $\kappa' \approx 6 \times 10^{-7} \text{ g cm}^{-4} \text{ K}^{-2}$ from fitting to Cassisi et al. (2007)’s opacities at $\rho = 2 \times 10^5 \text{ g cm}^{-3}$ and $T = 6 \times 10^6 \text{ K}$. When the core is isothermal with a constant c_P , the ther-

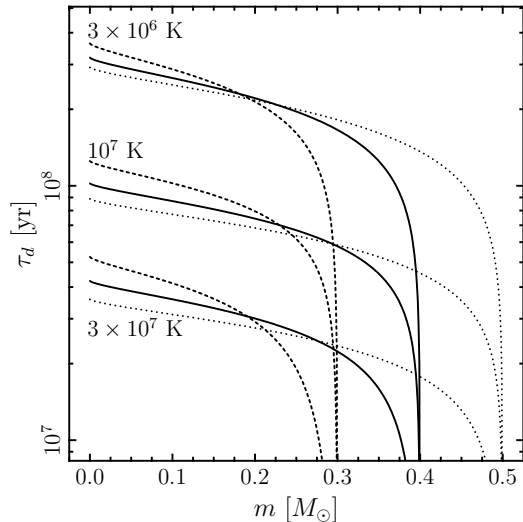


FIG. 2.— Thermal diffusion time from the outside of the core to interior mass points for $M = 0.3 M_{\odot}$ (dashed lines), $0.4 M_{\odot}$ (solid lines), and $0.5 M_{\odot}$ (dotted lines) He WDs. The isothermal core temperatures are marked.

mal diffusion time becomes

$$\begin{aligned} \tau_d &\approx \frac{3\kappa' c_P}{16a_{\text{SB}}cT_c} (r - r_0)^2 \\ &\approx 1.6 \times 10^8 \text{ yr} \left(\frac{\kappa'}{6 \times 10^{-7} \text{ g cm}^{-4} \text{ K}^{-2}} \right) \\ &\quad \times \left(\frac{6 \times 10^6 \text{ K}}{T_c} \right) \left(\frac{c_P}{3k_B/4m_p} \right) \left(\frac{r - r_0}{10^9 \text{ cm}} \right)^2, \quad (6) \end{aligned}$$

where we have normalized c_P to the dense liquid value for pure helium (i.e., an internal energy of $3k_B T$ per ion, where k_B is Boltzmann’s constant and m_p is the baryon mass).⁵

We numerically integrate equation (5) with the full dependences of κ and c_P for varying masses and isothermal temperature to find the thermal diffusion times from the core-envelope boundary to a given mass coordinate within the WD. These are shown in Figure 2 for $0.3 M_{\odot}$ (dashed lines), $0.4 M_{\odot}$ (solid lines), and $0.5 M_{\odot}$ (dotted lines) He WDs. Each set of lines shows different core temperatures. From top to bottom, these are 3×10^6 , 10^7 , and 3×10^7 K. The only dependence on M in equation (6) is from the radius of the core-envelope interface, which are all within 10–20% of each other for these low-mass WDs. Our simple estimate in equation (6) is fairly close to the integrated results in Figure 2; a core temperature of 6×10^6 K yields $\tau_d \approx 2 \times 10^8$ yr, and raising T_c by a factor of 10 decreases the thermal diffusion time by almost a factor of 10, as predicted by equation (6).

3.2. Numerical Evolution of the Thermal State for Constant \dot{M}

In this section, we describe several time-dependent calculations of constant \dot{M} onto a $0.4 M_{\odot}$ He WD in order to

⁵ For low-mass He WDs, the Coulomb coupling parameter Γ is ≈ 10 , so the ions are in a liquid state, but not necessarily deep into the $3k_B T$ limit. Thus, the actual values for c_P are between the ideal gas and liquid values.

discuss the thermal evolution and compare to the work of Townsley & Bildsten (2004). The specific outcomes for the \dot{M} histories appropriate to CVs calculated in §2.2 will be discussed in §4.

Numerical calculations were performed with the hydrodynamic Lagrangian stellar evolution code of Prialnik & Kovetz (1995), which contains an extended nuclear reaction network of 40 elements up to ^{31}P (Caughlan & Fowler 1988; Angulo et al. 1999; Timmes 1999) and implements the OPAL opacities (Iglesias & Rogers 1993, 1996). Convection is treated by mixing length theory with a mixing-length parameter $\alpha = 2$ (Mihalas 1978; Mazzitelli 1979; Vandenberg 1983). Inter-species diffusion is allowed to occur (see the Appendix for discussions of diffusion), but no other mixing processes are presumed. No ^3He is included in the newly accreted material (Shara 1980; Townsley & Bildsten 2004; Shen & Bildsten 2009a), but its presence in the incoming material should be negligible as the donor is unevolved. The CN mass-loss phase which follows the phase of rapid expansion uses a steady optically-thick supersonic wind solution (Prialnik 1986). Common envelope effects are neglected.

The $0.4 M_{\odot}$ He WD has a core composition of 98% He and 2% ^{14}N by mass and is surrounded with an initially thin envelope of solar composition. Three cases were studied, with different \dot{M} and initial T_c : $\dot{M} = 10^{-10}$ and $10^{-11} M_{\odot} \text{ yr}^{-1}$ for initial $T_c = 6 \times 10^6$ K, and $\dot{M} = 10^{-11} M_{\odot} \text{ yr}^{-1}$ for initial $T_c = 8 \times 10^6$ K. We numerically follow the evolution through hundreds of nova outbursts, with each nova cycle calculated through all evolutionary phases. Yaron et al. (2005) found that novae at these low accretion rates tend to erode the WD ($f > 1$). Therefore, after each outburst and resulting envelope ejection, the outer mass shell of the stripped WD core is split into multiple shells of $\lesssim 10^{-7} M_{\odot}$ so that the next nova cycle can be accurately calculated.

Equation (6) and Figure 2 indicate that the timescale for thermal coupling between the core and envelope is of order the timescale between nova outbursts for low $\dot{M} = 10^{-11} M_{\odot} \text{ yr}^{-1}$, although not for the higher $\dot{M} = 10^{-10} M_{\odot} \text{ yr}^{-1}$ case, which has a shorter accumulation time of $\approx 6 \times 10^6$ yr. However, because the envelope has a much lower mass (and thus a smaller thermal content) than the core, it will take many nova cycles to significantly increase T_c . The thermal content in the nearly ideal gas envelope of mass M_{env} with mean atomic weight $\mu \approx 0.6$ is $E_{\text{th,env}} = 3M_{\text{env}}k_B T/2\mu m_p \approx 4 \times 10^{45} \text{ erg} (T/10^7 \text{ K})(M_{\text{env}}/10^{-3} M_{\odot})$, whereas the thermal content in the He core is $E_{\text{th,core}} \approx 3Mk_B T_c/4m_p \approx 5 \times 10^{47} \text{ erg} (T_c/10^7 \text{ K})(M/0.4 M_{\odot})$. The 100-fold ratio of these thermal energies implies that it will take ~ 100 nova cycles to significantly heat the core if the only energy source is thermal. Some nuclear “simmering” could shorten the required time, as we discuss later in this section.

Figure 3 shows the time evolution of T_c for the three cases, all eventually reaching a final equilibrium core temperature. The core temperatures have been smoothed in order to make the evolution more clear. The dashed line is for $\dot{M} = 10^{-10} M_{\odot} \text{ yr}^{-1}$, which reaches an equilibrium temperature of $T_c \approx 9 \times 10^6$ K and sur-

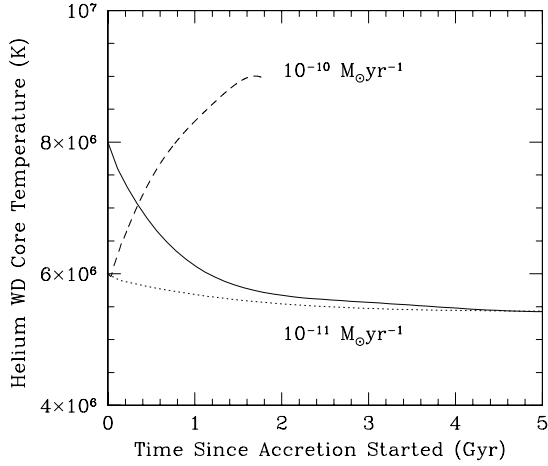


FIG. 3.— Time evolution of the core temperature, T_c , of the $0.4 M_\odot$ He WD for two different constant accretion rates and initial core temperatures. The solid (dotted) lines shows the $\dot{M} = 10^{-11} M_\odot \text{ yr}^{-1}$ case with initial core temperatures of 8×10^6 K (6×10^6 K). The dashed line is for an initial temperature of 6×10^6 K, but $\dot{M} = 10^{-10} M_\odot \text{ yr}^{-1}$. Lines are smoothed on a timescale of several nova cycles in order to make the secular evolution more clear.

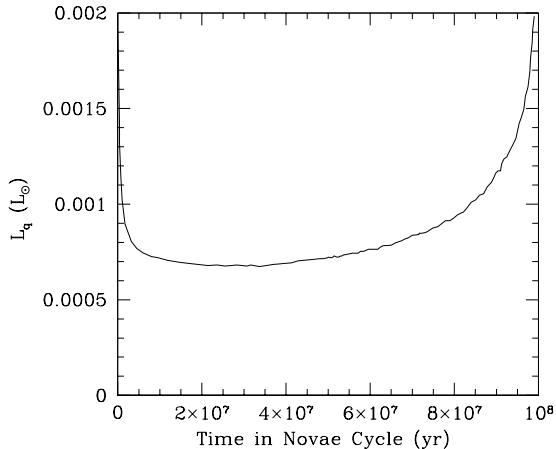


FIG. 4.— Time evolution of the quiescent surface luminosity, L_q , for a $0.4 M_\odot$ He WD accreting at $10^{-11} M_\odot \text{ yr}^{-1}$ after it has reached its equilibrium core temperature.

face luminosity in disk quiescence $L_q \approx 7 \times 10^{-3} L_\odot$. The time needed to reach this equilibrium is about that expected from the earlier considerations regarding the thermal content and heating of the core from the accumulated envelope, as $\approx 0.2 M_\odot$ of matter was put on the WD through this evolution, triggering 200 CNe.

The evolutions for lower $\dot{M} = 10^{-11} M_\odot \text{ yr}^{-1}$ are shown by the solid and dotted lines in Figure 3 for two different initial core temperatures. For these cases, the initial T_c is higher than the equilibrium value; accretion serves to slow the cooling of the WD as opposed to heating the core in the higher $\dot{M} = 10^{-10} M_\odot \text{ yr}^{-1}$ case. The equilibrium core temperature is $T_c = 5.5 \times 10^6$ K with a quiescent surface luminosity of $L_q \approx 7 \times 10^{-4} L_\odot$ for the majority of the accretion phase of each nova cycle, as shown in Figure 4, which plots the evolution of the quiescent surface luminosity during a typical nova cycle after the equilibrium core temperature has been reached.

Townsley & Bildsten (2004) and Epelstain et al. (2007) showed that equilibrium core temperatures would be reached under the action of accretion and CN events but did not consider WD masses this low. Townsley & Bildsten (2004) showed that the equilibrium core temperatures could be understood as that temperature where the cooling of the core (mostly during the accumulation stage) would be matched by the heating of the core (typically late in the accumulation, approaching the CN event). They highlighted two energy sources during accumulation: “compressional” heating (really entropy loss as material is advecting into the star) and slow nuclear burning. Following the derivation in Appendices A and B of Townsley & Bildsten (2004), which in turn follows Nomoto & Sugimoto (1977), Nomoto (1982), and Hernanz et al. (1988), yields the equivalent of Townsley & Bildsten (2004)’s equation (B4) for the “compressional” heating luminosity,

$$L_q \approx 4.5 \frac{k_B T_c}{m_p} \dot{M} \\ \approx 6.1 \times 10^{-4} L_\odot \left(\frac{T_c}{10^7 \text{ K}} \right) \left(\frac{\dot{M}}{10^{-11} M_\odot \text{ yr}^{-1}} \right), \quad (7)$$

after accounting for the differences in the Coulomb coupling parameter, mean atomic weight, and temperature in the core, and the larger M_{ign} . This predicts $L_{\text{comp}} = 3.4 \times 10^{-4} L_\odot$ and $L_{\text{comp}} = 5.5 \times 10^{-3} L_\odot$ for $\dot{M} = 10^{-11} M_\odot \text{ yr}^{-1}$ and $\dot{M} = 10^{-10} M_\odot \text{ yr}^{-1}$, respectively, after their equilibrium core temperatures have been reached. These estimates for the outgoing luminosity are $\approx 50\%$ lower than Figure 4 shows for $\dot{M} = 10^{-11} M_\odot \text{ yr}^{-1}$ and $\approx 20\%$ lower than the numerically calculated $L_q = 7 \times 10^{-3} L_\odot$ for $\dot{M} = 10^{-10} M_\odot \text{ yr}^{-1}$.

These differences in luminosity can be attributed to our numerical calculation’s inclusion of nuclear simmering. Townsley & Bildsten (2004) showed the potential of nuclear energy release during accumulation especially for massive envelopes like these (see their Figure 3). However they did not carry out this specific calculation. Our time dependent calculations allow us to see how the nuclear energy source can come into play.

Figure 5 shows snapshots of the thermal profile during different stages of the 10^8 yr CN cycle for $\dot{M} = 10^{-11} M_\odot \text{ yr}^{-1}$ after the WD has reached its equilibrium core temperature. The three dashed lines (top to bottom) are for times 5×10^6 yr, 7×10^6 yr and 10^7 yr, after the CN. The temperature inversion shows that heat flows from the hot post-CN envelope into the region beneath the burning layer during this time, to exit later during the first part of the accumulation phase. After this heat has been radiated away, the thermal profiles (three lower solid lines at 3×10^7 yr, 5×10^7 yr and 7×10^7 yr after the outburst) begin to resemble cooling WD profiles. Accumulation of material (and nuclear simmering) redevelops the temperature inversion (top solid line at 9×10^7 yr), and the dotted line shows the profile at 9.95×10^7 yr, when convection has initiated. Simply put, the excursions of the temperature during the CN event and the long accumulation time allow for some nuclear energy to be transported into the outer layers of the WD core over time, to be radiated later in the accumulation stage.

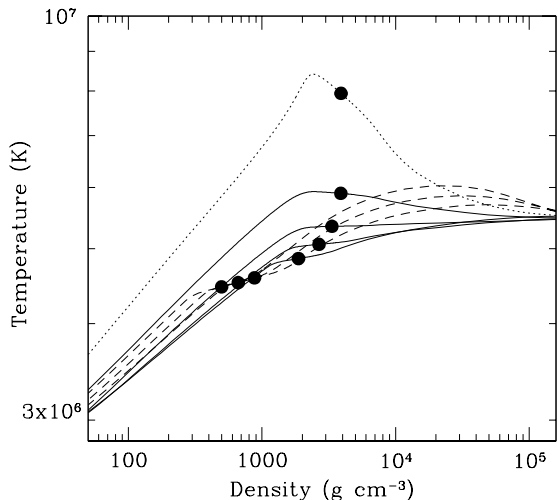


FIG. 5.— Density and temperature evolution during the period after a CN and the subsequent accumulation to the next explosion for a $0.4 M_{\odot}$ WD accreting at $\dot{M} = 10^{-11} M_{\odot} \text{ yr}^{-1}$. The three dashed lines are for times 5×10^6 yr, 7×10^6 yr, and 10^7 yr after the CN, from top to bottom. The solid lines, from bottom to top, are for times 3×10^7 yr, 5×10^7 yr, 7×10^7 yr, and 9×10^7 yr after the last outburst. The dotted line is the profile at a time of 9.95×10^7 yr, when convection has started. Bullets show the base of the accreted envelope.

4. THERMAL EVOLUTION FOR CV SCENARIOS AND DWARF NOVAE IN QUIESCENCE

As discussed in §2, stable mass transfer for low mass He WDs requires a low-mass companion that will transfer mass at the rate set by gravitational radiation losses. The more rapid mass transfer systems (i.e., above the period gap) that have stellar wind braking will be rarer. Our focus in this section is on the evolution of the two scenarios discussed in §2, building on the intuition gained in §3.

4.1. Thermal evolution

Figure 6 shows the mass accreted between nova outbursts (solid lines), envelope mass above the position where convection first begins during the thermonuclear runaway (dotted lines), and ejected mass (dashed lines) for scenarios A and B of Figure 1. Even though the mass transfer rates and core temperatures differ in these scenarios, the typical CN ignition masses change very little. Most importantly, diffusion of the H into the He and the resulting convection during the outburst lead to an ejected mass that is slightly larger than what was accreted. Hence, our earlier approximation that the accreted mass is ejected was appropriate.

The thermal evolution of the WD core is more complex due to the changing \dot{M} in these realistic scenarios, as shown in Figure 7. The top panel shows the T_c evolution for which the initial donor is a $0.2 M_{\odot}$ main sequence star (scenario A; solid line), which exhibits an initial heating to a near-equilibrium core temperature of $T_c = 6.8 \times 10^6$ K and a luminosity of $L_q \approx 2 \times 10^{-3} L_{\odot}$ (solid line in bottom panel) during the 4 Gyr when the accretion rate is nearly constant at $\dot{M} = 3 \times 10^{-11} M_{\odot} \text{ yr}^{-1}$; this value of L_q is in agreement with the prediction of Equation (7). This case is intermediate to the two calculations with constant \dot{M} discussed in §3.1. During these 4 Gyr, the

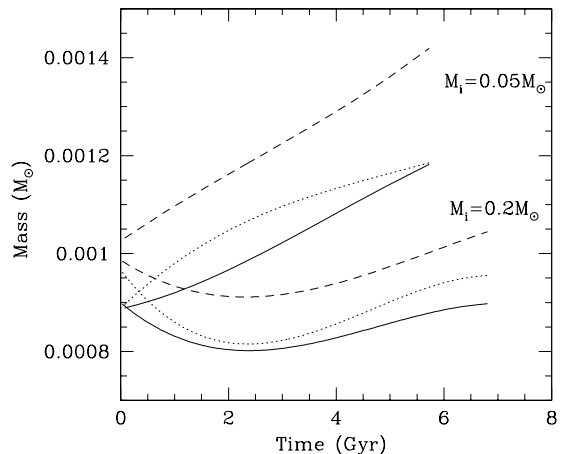


FIG. 6.— Accreted mass (solid lines), envelope mass above the position where convection first begins (dotted lines), and ejected mass (dashed lines) for the two binary evolution cases of Figure 1. Due to the diffusion of H into the He during accumulation, the initial convective envelope mass and ejected mass are always slightly larger than the amount of mass accreted since the last outburst.

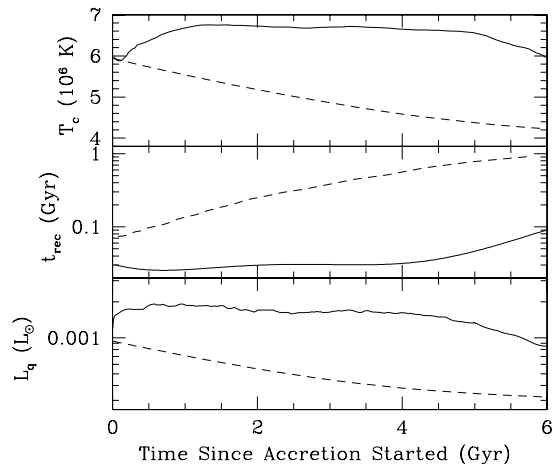


FIG. 7.— The top panel shows the mass-averaged WD core temperature as a function of time for a $0.4 M_{\odot}$ He WD with initial $T_c = 6 \times 10^6$ K for the two \dot{M} histories (scenarios A and B) of Figure 1. The solid (dashed) line is for initial $M_d = 0.2$ (0.05) M_{\odot} donor stars. The middle panel shows the time between CN outbursts for the same evolutionary scenarios. The bottom panel shows the evolution of the WD's surface luminosity in disk quiescence, L_q . For this plot, we use the minimum of L_q during each nova cycle, which because of the broad minimum is indicative of the 'typical' value (see Figure 4).

CN recurrence time (solid line in middle panel) is 3×10^7 years for about 130 CN events. After 4 Gyr, the donor begins to expand under further mass loss, and \dot{M} declines as the binary passes through the period minimum. The WD then cools, and the recurrence time becomes quite long.

The constantly declining \dot{M} of scenario B (where the initial donor is a $0.05 M_{\odot}$ brown dwarf) gives a different thermal outcome, as the WD constantly cools (dashed line in upper panel) and its luminosity declines (dashed line in bottom panel). There are only 25 CNE in 6 Gyr; indeed, the donor itself only has enough mass for about 50 CN events.

4.2. Dwarf novae in quiescence

Both of these scenarios have low enough \dot{M} that the accretion disk should be unstable, resulting in dwarf nova outbursts (Shafter 1992) and long periods of quiescence. When the accretion disk is in outburst, the accretion luminosity

$$\begin{aligned}
 L_{\text{acc}} &\approx \frac{GM\dot{M}}{2R} \\
 &\approx 0.004L_{\odot} \left(\frac{M}{0.4M_{\odot}} \right) \left(\frac{10^9 \text{ cm}}{R} \right) \\
 &\quad \times \left(\frac{\dot{M}}{10^{-11} M_{\odot} \text{ yr}^{-1}} \right) \quad (8)
 \end{aligned}$$

is an order of magnitude larger than the luminosity in the WD envelope, because the gravitational specific energy, GM/R , is much larger than the thermal specific energy, $kT_c/\mu m_p$, which sets the scale of the envelope’s thermal profile. However, when the disk is in quiescence, the excess L_{acc} is quickly radiated away on the thermal timescale near the WD’s photosphere, and the luminosity of the system is dominated by the WD’s quiescent surface luminosity, L_q , which originates from deep beneath the photosphere (Piro et al. 2005).

Ever since Sion (1999) discussed the value of T_{eff} measurements of dwarf novae in quiescence, observers and theorists have vigorously pursued this important diagnostic. Most recently, Townsley & Gänsicke (2009) summarized the observations and improved the earlier theoretical work (Townsley & Bildsten 2002; Godon & Sion 2002; Townsley & Bildsten 2003, 2005; Piro et al. 2005). In Figure 8, we have added the T_{eff} evolutions for our two scenarios to the original figure from Townsley & Gänsicke (2009). Some data are marginally consistent with the solid line (scenario A), whereas no observed WDs are as cold as predicted from our scenario B; however, it is unclear if the absence of these cold systems is physical or due to selection effects. It would be of interest to learn whether those cold systems near the solid line have any other evidence for having low-mass accretors.

The continual discoveries of CVs in quiescence by the Sloan Digital Sky Survey (e.g., Szkody et al. 2009; Gänsicke et al. 2009) and, in the near future, by SkyMapper (Murphy et al. 2008) will certainly provide new opportunities to reveal accreting He WDs. In particular, Gänsicke et al. (2009)’s recent discovery of the expected “pile-up” of CVs at the 80 – 86 min orbital period minimum has alleviated long-standing concerns regarding binary evolution. Hence, as we noted in the introduction, $\approx 20\%$ of the CVs in Gänsicke et al. (2009)’s compilation should harbor a He WD. The discovery and study of accreting WD pulsators (see Mukadam et al. 2007 for an updated list) may well be our best hope, as Arras et al. (2006) noted that low-mass WDs have colder effective temperatures for pulsation than higher mass WDs, and our T_{eff} calculations shown in Figure 8 are slightly colder than the blue edge calculated by Arras et al. (2006) for low gravity (e.g., low-mass WDs). Thus, a prevalence of pulsators at low T_{eff} may be an indicator of He WDs. Certainly more work is needed to make this connection clear, but the rapid increase in the

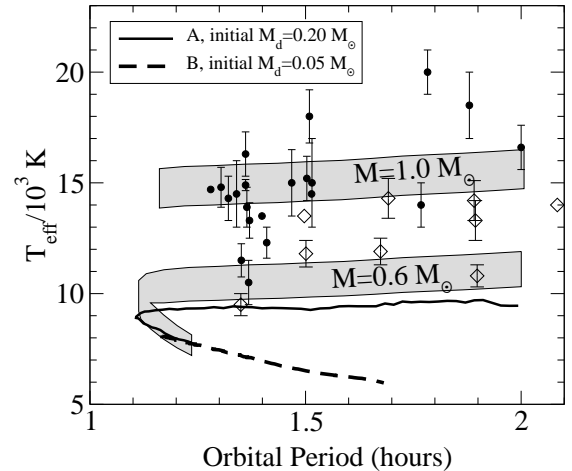


FIG. 8.— Adopted figure from Townsley & Gänsicke (2009). Solid (triangles) points are T_{eff} measurements from non-magnetic (magnetic) WDs in CVs below the period gap from Townsley & Gänsicke (2009). Shaded regions are the predicted effective temperatures found by Townsley & Gänsicke (2009) for $0.6 M_{\odot}$ and $1.0 M_{\odot}$ WDs. The solid and dashed lines are our calculations for a $0.4 M_{\odot}$ He WD with a $0.2 M_{\odot}$ and $0.05 M_{\odot}$ donor, respectively. We use the minimum in the quiescent surface luminosity for calculating T_{eff} . Figure 4 shows that for 90% of the CN cycle, the value of T_{eff} is no more than 15% higher than the value we plot.

discovery of such pulsators is bound to reveal a few new systems worthy of intensive study.

5. PHYSICS OF CLASSICAL NOVA OUTBURSTS

In the previous sections, we studied the secular evolution of the WD. We now turn our attention to details of the individual nova outbursts, focusing on the evolution of the convective burning phase, the composition of the nova ejecta, and the WD’s post-nova appearance as a supersoft x-ray source.

5.1. Evolution of the convective envelope and maximum temperatures

For most of the accretion phase of the nova cycle, the thermal profile is set by “compressional” heating (see §3.2). However, once the base of the envelope becomes dense and hot enough, the energy generation rate from nuclear burning becomes large enough that radiative diffusion can no longer effectively transport the luminosity. The radiative envelope is then transformed into a convective zone whose entropy is increased by continued nuclear burning until mass is lost via a radiatively-driven wind, and the nova outburst is observed. We now give a brief overview of the relevant physics during this stage of the CN evolution; for a more complete explanation of similar physics in He-burning convective envelopes, see §3 of Shen & Bildsten (2009b).

Figure 9 shows an example of the evolution of a convective envelope as it is heated by nuclear burning, numerically calculated for a $0.4 M_{\odot}$ WD that accreted mass at a rate of $10^{-11} M_{\odot} \text{ yr}^{-1}$ after it has reached its equilibrium core temperature of $5.5 \times 10^6 \text{ K}$. Dotted lines show temperature-density profiles of the envelope at 4.5×10^6 , 5900, and 0 yr before the convective zone reaches the top of our numerical grid, and solid lines show profiles 0.04 and 2.1 yr after this time, with more evolved envelopes at lower densities. The dashed line is the adiabatic slope

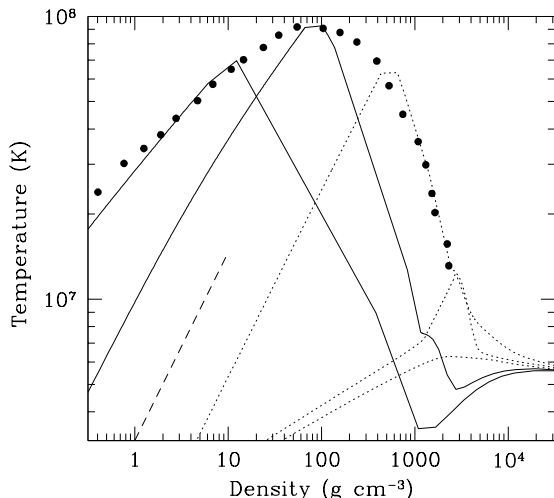


FIG. 9.— Density and temperature evolution during a CN outburst on a $0.4 M_{\odot}$ He WD. The dots display the evolution in time (from right to left) of the density and temperature at the base of the convective zone during the outburst. The uppermost dotted line is the profile when the convective zone reaches the surface of our numerical grid. The dotted lines beneath that are for times 5900 yr and 4.5×10^6 yr prior. The solid lines show the profile at times 0.04 (when the base temperature reaches its maximum) and 2.1 yr after convection reaches the surface. The dashed line is the adiabatic slope, $\partial \ln T / \partial \ln \rho|_s$, which is, as expected, nearly parallel to the convective region. The radial expansion of the outermost shell reduces the pressure at the base of the envelope, allowing for the underlying helium to adiabatically expand and cool (as is clear from the two solid lines at densities above 10^3 g cm^{-3}).

for an ideal gas, showing that the convective envelopes are indeed isentropic.

During the initial heating of the convective zone, the envelope is geometrically thin, with a scale height $h = P_b / \rho_b g$ much less than the WD radius R , and so the pressure at the base remains nearly constant: $P_b \approx GMM_{\text{env}} / 4\pi R^4$. Thus, as entropy is injected into the envelope during this phase, the temperature at the base increases and the density decreases while maintaining a constant pressure. Bullets in Figure 9 demarcate the base of the convective zone, which, as predicted, initially becomes less dense and hotter at constant pressure as the entropy increases.

Further entropy injection causes the scale height to grow until it becomes a significant fraction of the WD’s radius, and the envelope transitions to being geometrically thick. This leads to radial expansion of the envelope and a subsequent decrease in the base temperature. Thus, there is a maximum base temperature for the convective envelope, which depends only on M , M_{env} , and the envelope’s composition (Shen & Bildsten 2009b). For the model shown in Figure 9, the maximum temperature is $\approx 10^8 \text{ K}$.

Figure 10 shows analytic calculations of the maximum base temperature as a function of the convective envelope’s mass for a $0.4 M_{\odot}$ He core. The four lines are calculated with different hydrogen mass fractions, X , in order to parametrize the amount of core-envelope mixing. Increasing the helium abundance and thus the mean atomic weight μ decreases the number density of particles, and so T is higher for a given pressure. Doubling X decreases the maximum base temperature by $\approx 15\%$. Note that the temperatures for these models never reach

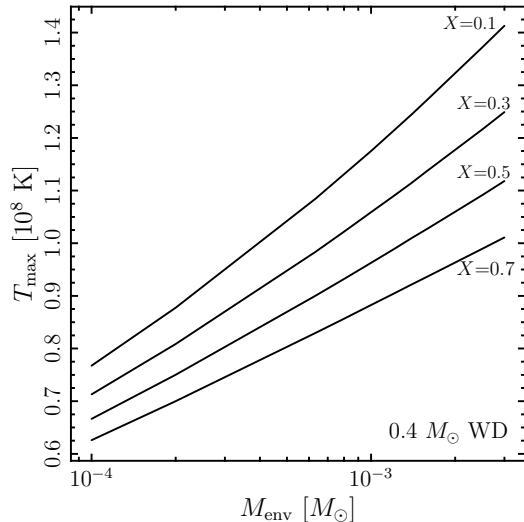


FIG. 10.— Maximum base temperatures vs. envelope mass for convective envelopes on a $0.4 M_{\odot}$ He WD. The curves are for different values of the hydrogen mass fraction, X , in the convective envelope, which depend on the amount of core-envelope mixing.

TABLE 2
CN EJECTA MASS FRACTIONS ON HE AND C/O WDS

Element	Solar	Ejecta (He WD)	Ejecta (C/O WD)
H	0.70	0.62	0.59
He	0.28	0.36	0.30
Z	0.017	0.021	0.11
^{12}C	3.9×10^{-3}	0.27×10^{-3}	2.3×10^{-3}
^{13}C	0.43×10^{-4}	0.87×10^{-4}	7.7×10^{-4}
^{14}N	0.10×10^{-2}	0.87×10^{-2}	5.7×10^{-2}
^{15}N	3.6×10^{-6}	0.28×10^{-6}	2.4×10^{-6}
^{16}O	0.94×10^{-2}	1.0×10^{-2}	4.8×10^{-2}
^{17}O	3.5×10^{-6}	1.4×10^{-3}	3.0×10^{-3}

values high enough to ignite the underlying He WD. Such an outcome would be exciting as it would likely lead to the birth of a He-burning star in a tight orbit.

5.2. Composition of the nova ejecta

Since the maximum base temperature in the convective envelope is not very high ($\approx 10^8 \text{ K}$), the main channels for nuclear burning during the outburst are the p - p chain and CNO cycle. While CNe on C/O WDs can dredge up large amounts of ^{12}C and ^{16}O nuclei from the underlying WD core, the only source of CNO nuclei for CNe on He WDs is from the accreted material and any trace CNO left in the He core. As a result, the ejecta has a metallicity, Z , close to the solar value, with an excess of H and He and a deficiency of ^{12}C and ^{16}O as compared to CNe on C/O WDs.

Table 2 shows the mass fractions for solar composition and for the numerically calculated ejecta of CNe on a $0.4 M_{\odot}$ He WD accreting at $\dot{M} = 10^{-11} M_{\odot} \text{ yr}^{-1}$ and a $0.65 M_{\odot}$ C/O WD accreting at $\dot{M} = 10^{-9} M_{\odot} \text{ yr}^{-1}$, computed after many nova cycles. Both calculations yield ejecta composed of $\sim 10\%$ core material and $\sim 90\%$ accreted material. This mixing results from the initiation of convection below the original core-envelope interface

due to diffusion during the accretion phase. However, because the cores are composed of different material, Z is essentially solar for CN ejecta on He cores with a CNO breakdown that roughly reflects the abundances of the equilibrium CNO cycle, whereas the ejecta from the C/O WD CN has a metallicity that is 5 times larger than solar with overabundances of all of the CNO elements. Note that the specific isotopic ratios depend strongly on the reaction rates that are used and should thus be regarded as a rough guide. However, the abundance trends of H, He, and metallicity are a robust result.

Classical novae whose ejecta exhibit near-solar metallicities, and enhanced He and CNO-processed abundances can thus help to identify these systems. Of the currently small number of ~ 25 CNe with measured ejecta abundances (for compilations, see Gehrz et al. 1998; Hachisu & Kato 2006), none definitively show these observational signatures. However, given the fact that there should be far fewer CNe from He WDs as compared to C/O WDs (see §6 for an estimate of the rates), this is not surprising.

5.3. Post-nova supersoft phase

During a nova outburst, mass is ejected from the convectively mixed envelope (containing both accreted and core material) via a radiatively-driven wind. This mass loss continues until the envelope re-establishes a hydrostatic solution, with a luminosity close to the red giant core mass-luminosity relation of Paczyński (1970). The H-rich envelope undergoes quasi-steady nuclear burning with a nearly constant luminosity, decreasing in mass as H is converted to He until the remaining envelope becomes too small to maintain a steady-state burning solution (Tuchman & Truran 1998; Sala & Hernanz 2005). For near-Eddington luminosity and a photospheric radius roughly equal to the radius of a $0.4 M_{\odot}$ core, the effective temperature yields a bright UV or supersoft x-ray source (Kahabka & van den Heuvel 1997) that lasts for as long as the envelope burns stably.

Specifying the core mass, envelope composition, and luminosity, and demanding hydrostatic equilibrium and continuity of the radius and pressure at the core-envelope interface uniquely determine M_{env} in this quasi-steady burning phase (see, e.g., Figs. 8 and 9 of Sala & Hernanz 2005 and Fig. 2 of Nomoto et al. 2007). As the envelope evolves, the luminosity remains nearly constant, decreasing slowly while T_{eff} increases and the envelope mass decreases until a minimum envelope mass is reached, which coincides with the maximum T_{eff} .

This initial phase of evolution is shown as solid lines in the H-R diagram in Figure 11 for He WD masses of 0.2, 0.25, 0.3, 0.4, and $0.5 M_{\odot}$. The evolution for these solutions begins to the right of the figure at the point where the photosphere is just inside the He WD's Roche radius assuming $M_d/M = 1/2$ and $P_{\text{orb}} = 4$ hr, which we take to be an estimate of the end of the mass-loss phase. The WD evolves towards the maximum T_{eff} and minimum M_{env} at the left. The equation of state (Saumon et al. 1995; Timmes & Swesty 2000; Rogers & Nayfonov 2002), opacity (Iglesias & Rogers 1993, 1996; Ferguson et al. 2005; Cassisi et al. 2007), electron screening (Graboske et al. 1973; Alastuey & Jancovici 1978; Itoh et al. 1979), nuclear burning network (Caughlan & Fowler 1988;

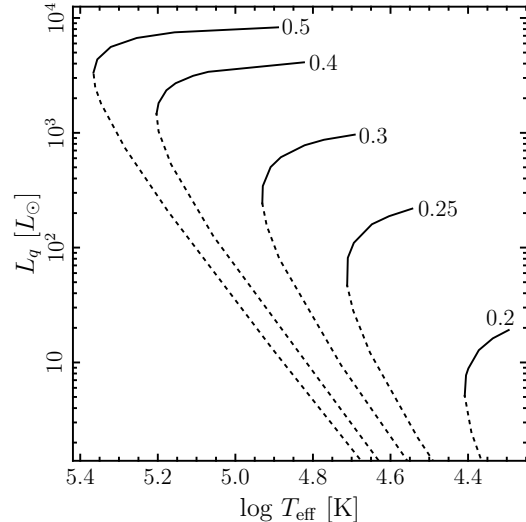


FIG. 11.— Evolution in the H-R diagram during the quasi-steady burning phase following a nova outburst. Each solid line shows the relation between L and T_{eff} for a stably burning model for He core masses of 0.2, 0.25, 0.3, 0.4, and $0.5 M_{\odot}$. Solid lines are truncated on the low T_{eff} side where the radius of the photosphere equals the Roche radius assuming a mass ratio of $1/2$ and $P_{\text{orb}} = 4$ hr. The dashed extensions are thermally unstable branches that are not physically realized.

Angulo et al. 1999; Timmes 1999), and neutrino cooling (Itoh et al. 1996) for these models are calculated with the MESA code package⁶ (Paxton et al., in prep.). The mass composition of the envelopes is 90% solar composition (as defined by Lodders 2003), which is accreted from the donor star, and 10% He core material due to convective mixing during the thermonuclear runaway, chosen to roughly match the ejecta abundances in Table 2. The CNO elements are assumed to be in chemical equilibrium as determined by their CNO-cycle burning rates, as their reaction timescales are shorter than the envelope's evolutionary timescale during this post-nova phase. Table 3 shows various properties of the envelope at the maximum T_{eff} and minimum M_{env} for several core masses, where τ_{SSS} is defined below, as well as the envelope mass at Roche lobe filling, $M_{\text{env,RL}}$. The maximum T_{eff} ranges from several to tens of eV.

While solutions exist for lower luminosities than that at the maximum T_{eff} and minimum M_{env} , these solutions are not physically relevant because they require the envelope mass to *increase* as time progresses (Sala & Hernanz 2005). Furthermore, a stability analysis shows that these solutions are thermally unstable (Paczynski 1983; Nomoto et al. 2007; Shen & Bildsten 2007). These unrealized solutions are shown as dashed lines in Figure 11. In reality, once the minimum envelope mass has been reached, nuclear burning declines, the envelope mass remains constant, and the WD evolves to the WD cooling track until accretion leads to the next nova outburst. Figure 12 shows the time evolution of the integrated nuclear luminosity in the envelope and the quiescent surface luminosity from our numeric calculation after a typical nova outburst. The quasi-constant luminosity phase lasts for ~ 1000 yr before burning declines.

⁶ <http://mesa.sourceforge.net/>

TABLE 3
POST-NOVA CONDITIONS AT MAXIMUM T_{eff} / MINIMUM M_{env}

M (M_{\odot})	$M_{\text{env,RL}}$ ($10^{-3} M_{\odot}$)	M_{env} ($10^{-3} M_{\odot}$)	L_q (L_{\odot})	T_{eff} (10^5 K)	τ_{SSS} (yr)
0.2	3.1	2.8	5.1	0.26	3.7×10^7
0.25	1.1	0.92	46	0.51	1.3×10^6
0.3	0.52	0.37	2.4×10^2	0.85	1.0×10^5
0.4	0.20	0.10	1.4×10^3	1.6	4.8×10^3
0.5	0.11	0.044	3.3×10^3	2.3	8.9×10^2

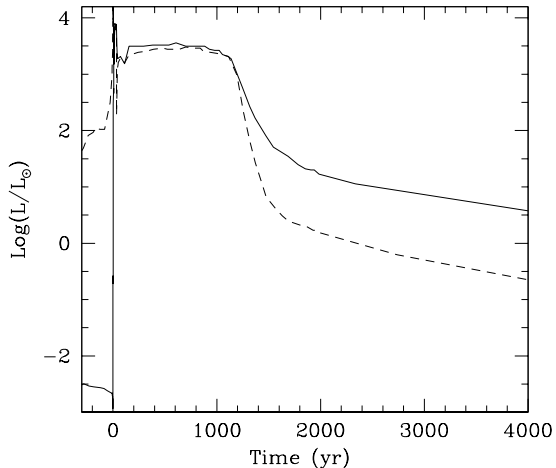


FIG. 12.— Integrated nuclear luminosity (dashed line) and quiescent surface luminosity, L_q , (solid line) versus time after a typical nova outburst on a $0.4 M_{\odot}$ He WD accreting at $10^{-11} M_{\odot} \text{ yr}^{-1}$ after it has reached its equilibrium T_c . The constant luminosity plateau lasts for ≈ 1000 yr, after which the nuclear luminosity drops sharply and the WD cools.

We define a characteristic time the evolved post-nova spends near its maximum T_{eff} as $\tau_{\text{SSS}} \equiv M_{\text{env}} E_{\text{nuc}} / L$, where $E_{\text{nuc}} \approx 4.1 \times 10^{18} \text{ erg g}^{-1}$ is the energy per mass obtained by converting H to He in material with $X = 0.68$. As shown in Table 3, these timescales are as long as 5000 yr for a $0.4 M_{\odot}$ core. Given this long duration, it is of interest to look for long-lasting ($\gtrsim 10$ yr) supersoft sources with short orbital periods < 4 hr. Possible systems like this are RX J0537.7-7034, which has $P_{\text{orb}} = 3.5$ hr and a dynamic mass estimate of $M = 0.4 - 0.8 M_{\odot}$ (Orio & Ogelman 1993; Greiner et al. 2000), and 1E 0035.4-7230 ($P_{\text{orb}} = 4.1$ hr; Orio et al. 1994; Schmidtke et al. 1996; van Teeseling et al. 1998), whose closest non-LTE spectral fit yields $T_{\text{eff}} \approx 3 \times 10^5$ K and $L \approx 2600 L_{\odot}$ (Kahabka et al. 1999), which is consistent with a $0.5 M_{\odot}$ He WD near its maximum T_{eff} . Neither of these sources seems to fit the canonical explanation of supersoft x-ray sources as thermal timescale mass transfer systems (King et al. 2001). Furthermore, Pietsch et al. (2005, 2007)’s growing catalog of M31 supersoft sources may also prove to be useful in this search for He WD post-nova supersoft x-ray sources.

6. CONCLUSIONS

Prompted by the lack of convincing detections of He WDs in CVs, we have studied their fate and thermal evolution in the hopes that observers may find new techniques with which to reveal or constrain this population.

We noted the existence of pre-CVs with He WDs in §2 and derived the mass-transfer evolution for two examples in §2.2, under the assumption of angular momentum loss due to gravitational wave radiation. In §3, we described the thermal evolution of the core both analytically and numerically for several cases with constant \dot{M} , and in §4, we described the reheating histories for the time-dependent CV evolutions of §2.2. In §5, we focused on the details of the individual nova events, describing the convective burning phase (§5.1), the ejecta composition (§5.2), and the post-CN outburst quasi-steady burning phase (§5.3).

In §4, we addressed the issue of the discovery of these systems while in quiescence. We now turn to the question of their detection via their nova outbursts and post-nova burning phases. From population synthesis predictions (de Kool 1992; Politano 1996; Howell et al. 2001), $\approx 20\%$ of CVs below the period gap harbor a He WD accretor. If, for simplicity, we consider only CNe on 0.4 and $0.6 M_{\odot}$ WDs, whose ignition masses differ by a factor of ≈ 2 for a given P_{orb} (Townsend & Bildsten 2005; Yaron et al. 2005), we find that the rate of CNe from He WDs is $\approx 10\%$ of all CNe with orbital periods below the period gap. However, for some novae, and especially extragalactic novae, the orbital period is much harder to measure, and so we cannot always divide the nova population into systems above and below the period gap. From theory and observations (Warner 2002; Townsend & Bildsten 2005), CNe below the period gap make up $10 - 25\%$ of all CNe, and thus we expect He WD accretors in $1 - 3\%$ of all CNe with no P_{orb} information. Note that this rough estimate does not take into account the selection effects that arise from the different peak luminosities and outburst timescales, which depend on the CV parameters.

As we showed in §5.3, the He WD remains bright in UV and supersoft x-rays during the post-nova burning phase. Due to the similar physics at play (i.e., H-burning on low-mass degenerate cores), these post-novae have similar observed characteristics to low-mass post-asymptotic giant branch (AGB) and post-early AGB stars. From Buzzoni et al. (2006) and references therein, the post-AGB birth rate is ~ 2 per yr in a $10^{11} M_{\odot}$ E/S0 galaxy. Extragalactic studies of CNe find a total rate of 20 ± 10 per yr in a galaxy of the same size (Williams & Shafter 2004), of which, from the calculation above, $0.2 - 0.6$ of these will be novae from He WDs. Thus, there should be $10 - 30\%$ as many post-novae He WDs as post-AGB stars.

As these post-novae cool, their evolution takes them towards the pulsational instability strip. Arras et al. (2006) examined the effect of envelope composition on

pulsating WDs, and found that above a helium mass fraction of ≈ 0.3 , a HeII convection zone is present that results in a second instability strip, with a hotter blue edge than the canonical H/HeI strip. If the post-nova envelope has a helium mass fraction of ≈ 0.4 due to core-envelope mixing, Arras et al. (2006) predict the blue edge of the resulting instability strip to be at $\approx 1.8 \times 10^4$ K, far hotter than the standard empirically-derived strip.

We thank Dean Townsley for a thorough review of a preliminary draft, Dina Prialnik and Attay Kovetz for use of their code, Boris Gänsicke, Tom Marsh, and Marina Orio for helpful discussions, and the referee for constructive comments. This work was supported by the National Science Foundation under grants PHY 05-51164 and AST 07-07633.

APPENDIX

Given the long accumulation timescales between novae on low-mass He WDs, we provide here an analytic estimate of the importance of chemical diffusion from the solar composition envelope into the He core. If the diffusion timescale, τ_d , is of order or less than the accumulation timescale, chemical diffusion will be non-negligible. In the limit that τ_d is much shorter than the accumulation timescale, the composition will be in a diffusive equilibrium governed by a balance of the gravitational and electric forces. For a degenerate He gas, the electric field is $e\vec{E} = -2m_p\vec{g}$, where \vec{g} is the gravitational acceleration, and so the net force on a hydrogen nucleus is $-m_p\vec{g}$. In diffusive equilibrium, balancing the forces yields an exponentially decreasing hydrogen tail going into the He core with a length scale roughly equal to the pressure scale height. Heavier elements like He, ^{12}C , ^{14}N , and ^{16}O , on the other hand, experience no net force in the degenerate core because they have the same charge-to-mass ratio as helium, and so they perform a random walk inwards and will have a constant mass fraction in the core when in diffusive equilibrium.

The timescale governing diffusion over a scale height is $\tau_d \sim H^2/D$, where $H = P/\rho g$ is the pressure scale height, and D is the diffusion coefficient. From Alcock & Illarionov (1980), the diffusion coefficient for ions in a perfect gas of background plasma is

$$D = \frac{3(2kT)^{5/2}}{16n_1(\pi m_1)^{1/2} Z_1^2 Z_i^2 e^4 \Lambda_i} \approx 1 \frac{\text{cm}^2}{\text{s}} \frac{T_7^{5/2} A_1^{1/2}}{\rho_3 Z_1^2 Z_i^2 \Lambda_i}, \quad (1)$$

where $\rho_3 = \rho/10^3 \text{ g cm}^{-3}$, T_7 is the temperature in units of 10^7 K, Z and A are the ion's charge and atomic weight, the Coulomb logarithm is Λ , the 1-subscript refers to the background ion, and the i -subscript refers to the diffusing ion species. For the case of a degenerate He core, the scale height is $H = 6.2 \times 10^6 \text{ cm } \rho_3^{2/3} (5/g_7)$, where g_7 is the gravitational acceleration at the core-envelope interface in units of 10^7 cm s^{-2} . For a $10^{-3} M_\odot$ envelope on a $0.4 M_\odot$ core, $g_7 \approx 5$.

The effects of electron degeneracy are accounted for in the Coulomb logarithm. For electron degenerate material,

$$\Lambda_i = \ln \left[1 + \frac{(kT)^3 \eta^{1/2} \exp(\eta)}{4\pi n_1 Z_1^3 Z_i^2 e^6} \right] = \ln \left[1 + 14.3 \frac{T_7^3 \eta^{1/2} \exp(\eta)}{\rho_3 Z_i^2} \right], \quad (2)$$

where η is the degeneracy parameter and the second line has been evaluated for a background of helium. The Coulomb ratio of Coulomb to thermal energies, $\Gamma_i \equiv E_{\text{Coulomb}}/E_{\text{thermal}}$, for He-He coupling near the outer edge of the core is $0.57\rho_3^{1/3}/T_7$, so the helium is roughly an ideal gas. With these approximations, the diffusion timescale through a scale height becomes

$$\tau_d \approx 2.4 \times 10^6 \text{ yr } \rho_3^{7/3} \left(\frac{5}{g_7} \right)^2 \frac{Z_i^2 \Lambda_i}{T_7^{5/2}}. \quad (3)$$

For a $10^{-3} M_\odot$ envelope halfway through its accumulation phase, the base temperature is 5×10^6 K, the density at the base is $3 \times 10^3 \text{ g cm}^{-3}$, and so the diffusion timescale for H into the He core is $\tau_d \approx 3 \times 10^8 \text{ yr}$, assuming $\eta = 2$. For carbon diffusing inwards, $\tau_d \approx 10^9 \text{ yr}$. Thus, for accumulation timescales $< 3 \times 10^8 \text{ yr}$, the composition profiles will not be in diffusive equilibrium.

Figure 13 shows the hydrogen (top panel) and helium (bottom panel) mass fractions as a function of pressure at different times during the 10^8 yr accumulation phase of a $0.4 M_\odot$ He WD accreting at a rate of $\dot{M} = 10^{-11} M_\odot \text{ yr}^{-1}$. From lower to higher pressure, these profiles are at times of 10^7 , 3×10^7 , 5×10^7 , 7×10^7 , and $9 \times 10^7 \text{ yr}$ after the previous CN. Because the accumulation timescale is 10^8 yr , neither the H nor heavier elements should be in diffusive equilibrium. Indeed, as Figure 13 shows, the H is not yet in diffusive equilibrium; its exponentially-decreasing tail extends only $\approx 50\%$ of a pressure scale height inwards.

REFERENCES

- Alastuey, A., & Jancovici, B. 1978, ApJ, 226, 1034
 Alcock, C., & Illarionov, A. 1980, ApJ, 235, 534
 Althaus, L. G., & Benvenuto, O. G. 1997, ApJ, 477, 313
 Angulo, C., et al. 1999, Nuclear Physics A, 656, 3
 Arras, P., Townsley, D. M., & Bildsten, L. 2006, ApJ, 643, L119
 Boschi, F., & Munari, U. 2004, A&A, 418, 869
 Buzzoni, A., Arnaboldi, M., & Corradi, R. L. M. 2006, MNRAS, 368, 877
 Cassisi, S., Potekhin, A. Y., Pietrinferni, A., Catelan, M., & Salari, M. 2007, ApJ, 661, 1094
 Caughlan, G. R., & Fowler, W. A. 1988, Atomic Data and Nuclear Data Tables, 40, 283
 de Kool, M. 1992, A&A, 261, 188

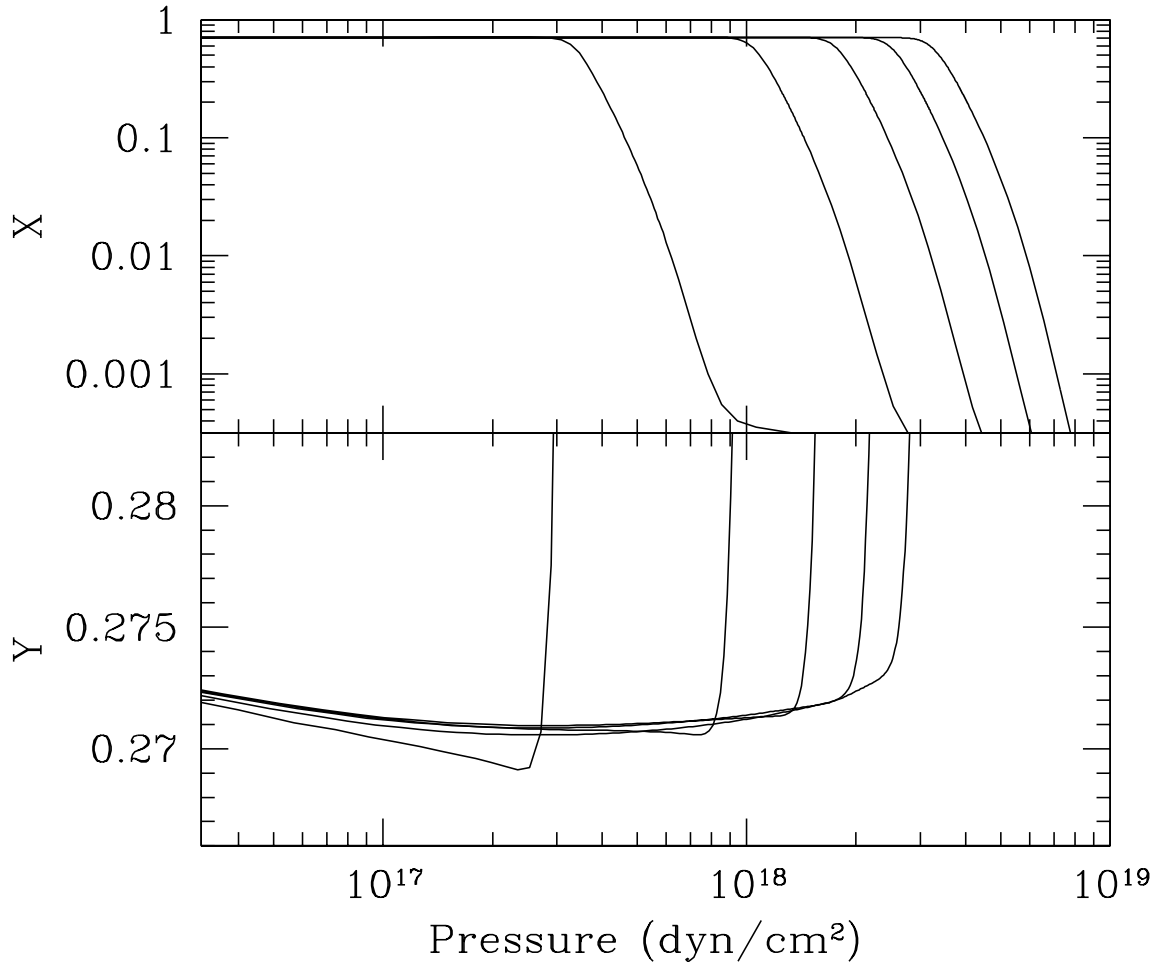


FIG. 13.— Hydrogen (top panel) and helium (bottom panel) mass fractions as a function of pressure for different times of an equilibrium CN cycle for $\dot{M} = 10^{-11} M_{\odot} \text{ yr}^{-1}$. From left to right, the curves are for times of 10%, 30%, 50%, 70%, and 90% of the 10^8 yr CN cycle. Note the different scales on the vertical axis.

- de Kool, M., & Ritter, H. 1993, *A&A*, 267, 397
Dominguez, I., Chieffi, A., Limongi, M., & Straniero, O. 1999, *ApJ*, 524, 226
Eggleton, P. P. 1983, *ApJ*, 268, 368
Epelstain, N., Yaron, O., Kovetz, A., & Prialnik, D. 2007, *MNRAS*, 374, 1449
Ferguson, J. W., Alexander, D. R., Allard, F., Barman, T., Bodnarik, J. G., Hauschildt, P. H., Heffner-Wong, A., & Tamanai, A. 2005, *ApJ*, 623, 585
Gänsicke, B. T. et al. 2009, *ArXiv e-prints*
Gehrz, R. D., Truran, J. W., Williams, R. E., & Starrfield, S. 1998, *PASP*, 110, 3
Godon, P., & Sion, E. M. 2002, *ApJ*, 566, 1084
Graboske, H. C., Dewitt, H. E., Grossman, A. S., & Cooper, M. S. 1973, *ApJ*, 181, 457
Greiner, J., Orio, M., & Schwarz, R. 2000, *A&A*, 355, 1041
Hachisu, I., & Kato, M. 2006, *ApJS*, 167, 59
Heney, L., & L'Ecuyer, J. 1969, *ApJ*, 156, 549
Hernanz, M., Isern, J., Canal, R., Labay, J., & Mochkovitch, R. 1988, *ApJ*, 324, 331
Hjellming, M. S., & Webbink, R. F. 1987, *ApJ*, 318, 794
Howell, S. B., Nelson, L. A., & Rappaport, S. 2001, *ApJ*, 550, 897
Iben, I. J., Fujimoto, M. Y., & MacDonald, J. 1992, *ApJ*, 388, 521
Iben, I. J., & Tutukov, A. V. 1992, *ApJ*, 389, 369
—, 1993, *ApJ*, 418, 343
Iglesias, C. A., & Rogers, F. J. 1993, *ApJ*, 412, 752
—, 1996, *ApJ*, 464, 943
Itoh, N., Hayashi, H., Nishikawa, A., & Kohyama, Y. 1996, *ApJS*, 102, 411
Itoh, N., Totsuji, H., Ichimaru, S., & Dewitt, H. E. 1979, *ApJ*, 234, 1079
Kahabka, P., Parmar, A. N., & Hartmann, H. W. 1999, *A&A*, 346, 453
Kahabka, P., & van den Heuvel, E. P. J. 1997, *ARA&A*, 35, 69
King, A. R., Schenker, K., Kolb, U., & Davies, M. B. 2001, *MNRAS*, 321, 327
Kolb, U., & Baraffe, I. 1999, *MNRAS*, 309, 1034
Lodders, K. 2003, *ApJ*, 591, 1220
Marsh, T. R., Dhillon, V. S., & Duck, S. R. 1995, *MNRAS*, 275, 828
Maxted, P. F. L., Marsh, T. R., Moran, C., Dhillon, V. S., & Hilditch, R. W. 1998, *MNRAS*, 300, 1225
Maxted, P. F. L., Napiwotzki, R., Dobbie, P. D., & Burleigh, M. R. 2006, *Nature*, 442, 543
Maxted, P. F. L., O'Donoghue, D., Morales-Rueda, L., Napiwotzki, R., & Smalley, B. 2007, *MNRAS*, 376, 919
Mazzitelli, I. 1979, *A&A*, 79, 251
Mihalas, D. 1978, in *Stellar Atmospheres*, 2nd (San Francisco, CA: W. H. Freeman and Co.)
Mukadam, A. S., Gänsicke, B. T., Szkody, P., Aungwerojwit, A., Howell, S. B., Fraser, O. J., & Silvestri, N. M. 2007, *ApJ*, 667, 433
Murphy, S. J., Keller, S. C., Schmidt, B., Tisserand, P., Bessell, M., Francis, P., & Da Costa, G. 2008, *ArXiv e-prints*
Nebot Gómez-Morán, A. et al. 2009, *A&A*, 495, 561
Nomoto, K. 1982, *ApJ*, 253, 798
Nomoto, K., Saio, H., Kato, M., & Hachisu, I. 2007, *ApJ*, 663, 1269
Nomoto, K., & Sugimoto, D. 1977, *PASJ*, 29, 765
Orio, M., della Valle, M., Massone, G., & Ogelman, H. 1994, *A&A*, 289, L11
Orio, M., & Ogelman, H. 1993, *A&A*, 273, L56+
Paczynski, B. 1967, *Acta Astronomica*, 17, 287
—, 1970, *Acta Astronomica*, 20, 47
Paczynski, B. 1983, *ApJ*, 264, 282
Paquette, C., Pelletier, C., Fontaine, G., & Michaud, G. 1986, *ApJS*, 61, 177
Patterson, J. 2001, *PASP*, 113, 736

- Pietsch, W., Fliri, J., Freyberg, M. J., Greiner, J., Haberl, F., Riffeser, A., & Sala, G. 2005, *A&A*, 442, 879
- Pietsch, W. et al. 2007, *A&A*, 465, 375
- Piro, A. L., Arras, P., & Bildsten, L. 2005, *ApJ*, 628, 401
- Politano, M. 1996, *ApJ*, 465, 338
- Prialnik, D. 1986, *ApJ*, 310, 222
- Prialnik, D., & Kovetz, A. 1995, *ApJ*, 445, 789
- Pyrzas, S. et al. 2009, *MNRAS*, 394, 978
- Rebassa-Mansergas, A. et al. 2008, *MNRAS*, 390, 1635
- Ribas, I., Morales, J. C., Jordi, C., Baraffe, I., Chabrier, G., & Gallardo, J. 2008, *Memorie della Societa Astronomica Italiana*, 79, 562
- Rich, R. M., Mould, J., Picard, A., Frogel, J. A., & Davies, R. 1989, *ApJ*, 341, L51
- Rogers, F. J., & Nayfonov, A. 2002, *ApJ*, 576, 1064
- Sala, G., & Hernanz, M. 2005, *A&A*, 439, 1061
- Salaris, M., Cassisi, S., & Weiss, A. 2002, *PASP*, 114, 375
- Sandquist, E. L., Taam, R. E., & Burkert, A. 2000, *ApJ*, 533, 984
- Saumon, D., Chabrier, G., & van Horn, H. M. 1995, *ApJS*, 99, 713
- Schmidtke, P. C., Cowley, A. P., McGrath, T. K., Hutchings, J. B., & Crampton, D. 1996, *AJ*, 111, 788
- Schreiber, M. R., & Gänsicke, B. T. 2003, *A&A*, 406, 305
- Serenelli, A. M., & Fukugita, M. 2005, *ApJ*, 632, L33
- Shafter, A. W. 1992, *ApJ*, 394, 268
- Shara, M. M. 1980, *ApJ*, 239, 581
- Shara, M. M., Livio, M., Moffat, A. F. J., & Orio, M. 1986, *ApJ*, 311, 163
- Shara, M. M., Prialnik, D., & Kovetz, A. 1993, *ApJ*, 406, 220
- Shen, K. J., & Bildsten, L. 2007, *ApJ*, 660, 1444
- . 2009a, *ApJ*, 692, 324
- . 2009b, *ApJ*, 699, 1365
- Sion, E. M. 1999, *PASP*, 111, 532
- Starrfield, S., Truran, J. W., Sparks, W. M., & Kutter, G. S. 1972, *ApJ*, 176, 169
- Stehle, R., Kolb, U., & Ritter, H. 1997, *A&A*, 320, 136
- Steinfadt, J. D. R., Bildsten, L., & Howell, S. B. 2008, *ApJ*, 677, L113
- Sweigart, A. V., Greggio, L., & Renzini, A. 1989, *ApJS*, 69, 911
- Szkody, P. et al. 2009, *AJ*, 137, 4011
- Thomas, H.-C. 1967, *Z. Astrophys.*, 67, 420
- Timmes, F. X. 1999, *ApJS*, 124, 241
- Timmes, F. X., & Swesty, F. D. 2000, *ApJS*, 126, 501
- Townsley, D. M., & Bildsten, L. 2002, *ApJ*, 565, L35
- . 2003, *ApJ*, 596, L227
- . 2004, *ApJ*, 600, 390
- . 2005, *ApJ*, 628, 395
- Townsley, D. M., & Gänsicke, B. T. 2009, *ApJ*, 693, 1007
- Tuchman, Y., & Truran, J. W. 1998, *ApJ*, 503, 381
- Vandenberg, D. A. 1983, *ApJS*, 51, 29
- van Teeseling, A., Reinsch, K., Pakull, M. W., & Beuermann, K. 1998, *A&A*, 338, 947
- Warner, B. 2002, in *American Institute of Physics Conference Series*, Vol. 637, *Classical Nova Explosions*, ed. M. Hernanz & J. José, 3–15
- Webbink, R. F. 1985, *Stellar evolution and binaries* (Cambridge University Press), 39–+
- Williams, S. J., & Shafter, A. W. 2004, *ApJ*, 612, 867
- Yaron, O., Prialnik, D., Shara, M. M., & Kovetz, A. 2005, *ApJ*, 623, 398